Black Hole Superradiant Instability from Ultralight Spin-2 Fields

Richard Brito,[1,*] Sara Grillo,[2,1] and Paolo Pani[1,†]
[1]Dipartimento di Fisica, "Sapienza" Università di Roma and Sezione INFN Roma1, Piazzale Aldo Moro 5, 00185 Roma, Italy
[2]Dipartimento di Fisica G. Occhialini, Università degli Studi di Milano Bicocca, Piazza della Scienza 3, 20126 Milano, Italy

(Received 15 February 2020; revised manuscript received 9 April 2020; accepted 6 May 2020; published 27 May 2020)

Ultralight bosonic fields are compelling dark-matter candidates and arise in a variety of beyond standard model scenarios. These fields can tap energy and angular momentum from spinning black holes through superradiant instabilities, during which a macroscopic bosonic condensate develops around the black hole. Striking features of this phenomenon include gaps in the spin-mass distribution of astrophysical black holes and a continuous gravitational-wave (GW) signal emitted by the condensate. So far these processes have been studied in great detail for scalar fields and, more recently, for vector fields. Here we take an important step forward in the black hole superradiance program by computing, analytically, the instability timescale, direct GW emission, and stochastic background, in the case of massive tensor (i.e., spin-2) fields. Our analysis is valid for any black hole spin and for small boson masses. The instability of massive spin-2 fields shares some properties with the scalar and vector cases, but its phenomenology is much richer, for example, there exist multiple modes with comparable instability timescales, and the dominant GW signal is hexadecapolar rather than quadrupolar. Electromagnetic and GW observations of spinning black holes in the mass range $M \in (1, 10^{10})\, M_\odot$ can constrain the mass of a putative spin-2 field in the range $10^{-22} \lesssim m_b\, c^2/\mathrm{eV} \lesssim 10^{-10}$. For $10^{-17} \lesssim m_b\, c^2/\mathrm{eV} \lesssim 10^{-15}$, the space mission *LISA* could detect the continuous GW signal for sources at redshift $z = 20$, or even larger.

DOI: 10.1103/PhysRevLett.124.211101

Introduction.—In the last decade, a surprising connection between gravity in the strong field regime and particle physics has emerged in several contexts [1–3]. Probably the most spectacular one is the possibility to search for ultralight bosons with current [1,4–9] and future [10–13] gravitational-wave (GW) detectors. Ultralight bosons (such as the QCD axion, axionlike particles, dark photons, etc.) could be a significant component of the dark matter [1,14–16] and are predicted in a multitude of beyond standard model scenarios [14,16–18], including extra dimensions and string theories. They naturally interact very weekly and in a model-dependent fashion with baryonic matter, but their gravitational interaction is universal.

A striking gravitational effect triggered by these fields near spinning black holes (BHs) is the superradiant instability [19–23], which occurs whenever the boson frequency ω_R satisfies the superradiant condition $0 < \omega_R < m\Omega_H$, where Ω_H is the horizon angular velocity and m is the azimuthal quantum number of the unstable mode.

Recent years have witnessed spectacular progress in understanding superradiant instabilities and their phenomenology, both for scalars [4–7,20,24–26] and for vectors [27–37]. In the superradiant regime, the BH spins down, transferring energy and angular momentum to a mostly dipolar ($m = 1$) boson condensate until $\omega_R \sim \Omega_H$. The condensate is then dissipated through the emission of mostly quadrupolar GWs, with frequency set by the boson mass $m_b \equiv \mu\hbar$ (we use $G = c = 1$ units). On longer timescales this process continues for $m > 1$ modes. The mechanism is most effective when the boson's Compton wavelength is comparable to the BH's gravitational radius, i.e., when the "gravitational coupling" $\alpha \equiv M\mu = \mathcal{O}(0.1)$, which requires $m_b \sim 10^{-11}\ (M_\odot/M)\,\mathrm{eV}$ [22].

Compared to the scalar and vector cases, very little is known about the much more involved problem of the superradiant instability triggered by massive tensor (i.e., spin-2) fields. To the best of our knowledge the only work on the subject performed a perturbative expansion to linear order in the spin [38], which is inaccurate in the most interesting regime of highly spinning BHs. Furthermore, the coupling of a massive spin-2 field to gravity is highly nontrivial [39–43] and this increases the complexity of the problem. In this Letter, we fill a gap in the BH superradiance program by computing analytically for the first time the superradiant instability timescale and the GW emission from BH condensates made of massive spin-2 fields. We work in the "small-coupling" limit $\alpha \ll 1$, but do not make any assumption on the BH spin. As we shall argue, the phenomenology of the spin-2 superradiant instability is similar to the spin-1 case, leading to exquisite constraints on beyond standard model tensor fields. Furthermore, novel effects occur in the spin-2 case that are absent for scalars and vectors.

Massive spin-2 fields around spinning BHs.—A massive tensor field cannot be trivially coupled to gravity [39,43]

and, at the nonlinear level, there is a unique way to couple two dynamical tensors [40–42]. On a curved, Ricci-flat [44] spacetime g_{ab}, the unique action to cubic order in the spin-2 fields has been derived in Ref. [45] and schematically reads

$$S^{(3)} = \int d^4x\sqrt{-g}\Big[\mathcal{L}_{\rm GR}(G) + \mathcal{L}_{\rm GR}(H) - \frac{\mu^2}{4}(H_{ab}H^{ab} - H^2) + \mathcal{L}_{\rm cubic}(G,H)\Big], \quad (1)$$

where G_{ab} and H_{ab} are the canonically normalized mass eigenstates describing a massless and a massive spin-2 field, respectively, $\mathcal{L}_{\rm GR}$ is the Einstein-Hilbert Lagrangian truncated at quadratic order, $\mathcal{L}_{\rm cubic}$ (to be discussed in the Supplemental Material [46]) is a complicated interaction term that depends either linearly on G_{ab} and quadratically on H_{ab}, or cubically on G_{ab} and H_{ab} independently.

To the zeroth order in the massive field H_{ab}, the field equations reduce to $R_{ab}(g) = 0$ and we consistently assume a background Kerr metric, although our computation does not depend on the details of the background and should be valid also for different solutions that might exist in bimetric theories [50,51]. To first order, the linearized field equations describing the five physical degrees of freedom of a massive spin-2 perturbation read [38,52]

$$\Box H_{ab} + 2R_{acbd}H^{cd} - \mu^2 H_{ab} = 0, \quad (2)$$

$$\nabla^a H_{ab} = 0, \qquad H^a{}_a = 0, \quad (3)$$

where the box operator, the Riemann tensor, and contractions are constructed with the background metric.

Although Eqs. (2) and (3) are not separable on a Kerr background with standard methods, they can be solved in the $\alpha \ll 1$ limit to compute the spectrum of unstable modes, as detailed in the Supplemental Material. Our method is based on matched asymptotics, namely, the field equations are solved separately in a far zone ($r \gg M$) and in a near zone ($r \ll \mu^{-1}$). The two solutions can be matched in a common region when $\alpha \ll 1$, see Fig. 1.

In addition, at variance with the scalar and vector cases, to be able to solve the field equations analytically we also need to consider the region where the Riemann tensor term in Eq. (2) is much smaller than the mass term. This requires [53]

$$r \gg r_C \equiv M\alpha^{-2/3}. \quad (4)$$

Since $M \ll r_C \ll 1/\mu$ in the small-coupling limit, the matching region satisfies the above condition. Because of condition (4), our method fails to capture eigenfunctions with significant support at $r \lesssim r_C$. This is the case for the unstable spherical mode that exists in the nonspinning case [38,50,54] and for the "special" dipole mode found numerically in Ref. [38] (see [55]). On the other hand, as we will check *a posteriori*, the ordinary superradiant eigenfunctions have significant support only around the Bohr radius, $r_{\rm Bohr} \sim M/\alpha^2$ [22], and are therefore well reproduced by our analytical approximation.

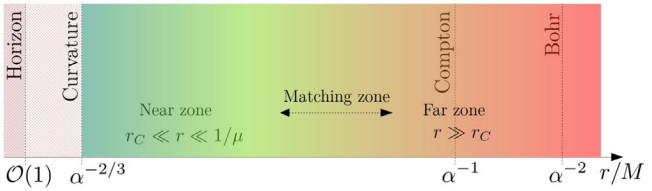

FIG. 1. Schematic representation of the length scales involved in the superradiant instability of massive spin-2 fields. In the small-coupling ($\alpha \equiv M\mu \ll 1$) limit, all scales are well separated from each other. Our approximation fails to capture solutions with significant support within the curvature radius, $r_C = M/\alpha^{2/3}$. The standard superradiant modes instead have significant support around the Bohr radius, $r_{\rm Bohr} = M/\alpha^2$, the largest scale in the problem.

In the far region, the tensor H_{ab} can be decomposed in a basis of "pure-orbital" tensor spherical harmonics [56–58]. The radial dependence is entirely encoded in the hydrogenlike radial equation, whose eigenfunctions can be labeled by their orbital angular momentum $\ell \geq 0$ and by the overtone number $n \geq 0$ representing the number of nodes in the radial function. The energy levels are

$$\omega_R \simeq \mu\left(1 - \frac{\alpha^2}{2(\ell+n+1)^2}\right), \quad (5)$$

as in the scalar and vector cases.

The instability timescale $\tau_{\rm inst}$ can be computed through the energy decay rate, $\Gamma = \dot{E}_H/M_c = 1/\tau_{\rm inst}$, where M_c is the energy of the condensate and $\dot{E}_H$ is the energy flux across the horizon, which can, in turn, be computed through the stress-energy tensor stemming from action (1) [45,59] and explicitly given in the Supplemental Material [46]. By also making use of the BH absorption probability for long-wavelength massless spin-2 waves [22,60,61], the computation detailed in the Supplemental Material yields

$$\Gamma = -C_{j\ell}\frac{\mathcal{P}_{jm}(\chi)}{\mathcal{P}_{jm}(0)}\alpha^{2(\ell+j)+5}(\omega_R - m\Omega_{\rm H}), \quad (6)$$

where

$$\mathcal{P}_{jm}(\chi) = (1+\Delta)\Delta^{2j}\prod_{q=1}^{j}\left[1 + 4M^2\left(\frac{\omega_R - m\Omega_{\rm H}}{q\kappa}\right)^2\right] \quad (7)$$

is proportional to the BH absorption probability, $\Delta = \sqrt{1-\chi^2}$, and $\kappa = [\Delta/(1+\Delta)]$. The integer $j \in (|\ell-2|, \ell+2) \geq 0$ is the total angular momentum, the integer $m \in (-j, j)$, and the constant $C_{j\ell}$ depends on the mode. The superradiant instability requires a nonaxisymmetric

mode ($m \neq 0$) and therefore $j \geq 1$. Hence, at variance with the scalar and vector cases, there exist *two* dominant unstable modes with the same scaling $\tau_{\rm inst} \sim -\alpha^{-9}(\omega_R - m\Omega_H)^{-1}$: the dipole $j = \ell = 1$, and the quadrupole $j = 2$, $\ell = 0$ (the latter being absent in the scalar and vector cases). We find $C_{20} = 128/45$ and $C_{11} = 10/9$, so that the quadrupole mode has always the shortest instability timescale. When the BH spin is small, the analytical results match very well the numerical ones obtained in Ref. [38] to linear order in the spin.

GWs from spin-2 condensates around BHs.—The GW dissipation timescale $\tau_{\rm GW}$ can be computed from the stress-energy tensor of the condensate. Crucially, $\tau_{\rm GW} \gg \tau_{\rm inst} \gg M$ in the small-coupling limit, so the process can be thought to occur in two stages [32,62]. In the first (linear) phase, the condensate grows on a timescale given by $\tau_{\rm inst} = 1/\Gamma$ for the most unstable modes [see Eq. (6)] until the superradiant condition $\omega_R \sim m\Omega_H$ is nearly saturated. In the second (nonlinear) phase, GW emission governs the evolution of the condensate, which is dissipated over the timescale $\tau_{\rm GW} \gg \tau_{\rm inst}$. This separation of scales allows us to study the process in a quasiadiabatic approximation [32,62] using Teukolsky's formalism to compute the GW emission [63,64]. As detailed in the Supplemental Material [46], in the small-frequency limit the GW flux $\dot{E}_{\rm GW}$ can be computed analytically [62,65,66]. For the most unstable modes, we get

$$\tau_{\rm GW} \equiv \frac{M_c}{\dot{E}_{\rm GW}} \sim D_{j\ell m}\frac{M^2}{M_c}\alpha^{-4\ell-10} \sim 290\left(\frac{0.2}{\alpha}\right)^{10}\ {\rm s}, \quad (8)$$

where M_c is the mass of the particular mode, $D_{202} \approx 2 \times 10^{-2}$, and $D_{111} \approx 2.6$ (their analytical form is given in the Supplemental Material). As a useful estimate, in the last step we assumed $M_c \sim 0.1M$ [62], $M \sim 30\ M_\odot$, and $\ell = 0$, showing that $\tau_{\rm GW} \gg \tau_{\rm inst}$ can be relatively short.

The presence of two unstable modes with comparable timescales slightly complicates the above picture. The dipolar mode grows until $\Omega_H = \omega_R$, reaching a mass $M_c^{m=1}$. At the same time, the BH spin keeps being extracted by the quadrupolar mode, which is still unstable in this regime and indeed saturates only at $\Omega_H = \omega_R/2$, reaching a mass $M_c^{m=2}$. When the BH spins down such that $\Omega_H < \omega_R$, the dipole mode leaves the superradiant regime and is quickly reabsorbed by the BH (since the absorption timescale is significantly shorter than that of GW emission), thus giving back almost all its mass and spin [66]. Therefore, at the time when $\Omega_H = \omega_R/2$, the net mass and angular momentum loss are entirely due to the quadrupole mode, which is finally emitted in GWs over the timescale in Eq. (8).

The emitted signal is nearly monochromatic, with frequency $f_s = \omega_R/\pi$, where ω_R is given in Eq. (5). Thus, BH-boson condensates are continuous sources, like pulsars for the Laser Interferometer Gravitational Wave Observatory (LIGO) and Virgo or verification binaries for Laser Interferometer Space Antenna (*LISA*). There are, however, two notable differences: (i) Depending on the value of α, the GW emission timescale $\tau_{\rm GW}$ can be significantly shorter than the observation time, resulting in an impulsive signal. (ii) At variance with the case of massive scalar and vector fields, GW emission for the dominant spin-2 mode is mostly *hexadecapolar* and not quadrupolar, since it is produced by a spinning quadrupolar field and not by a spinning dipolar field. The hexadecapolar nature of the radiation implies that the signal vanishes along the BH spin axis, at variance with the quadrupolar case, for which it is maximum in that direction.

To estimate the GW signal, we define the characteristic GW amplitude as

$$h_c = \sqrt{N_{\rm cycles}}h_{\rm rms}, \quad (9)$$

where $N_{\rm cycles} \sim \min[\sqrt{fT_{\rm obs}}, \sqrt{f_s\tau_{\rm GW}}]$ is the approximate numbers of cycles in the detector, $f = f_s/(1+z)$ is the detector frame frequency, $T_{\rm obs}$ is the observation time, and $h_{\rm rms} = \sqrt{\dot{E}_{\rm GW}/(5f^2r^2\pi^2)}$ is the root-mean-square amplitude obtained by averaging over source and detector orientations (see Refs. [6,7] for details).

Bounds from BH mass-spin distribution.—We can now turn our attention to the phenomenology of the BH superradiant instability for massive spin-2 fields. A generic prediction is that highly spinning BHs would lose angular momentum over a timescale $\tau_{\rm inst} = 1/\Gamma$ [see Eq. (6)] that might be much shorter than typical astrophysical timescales. Thus, an indirect signature of ultralight bosons is statistical evidence for slowly rotating BHs in a part of the Regge (mass versus angular momentum) plane of astrophysical BHs [6,7,22,33,67–69].

Our results are summarized in Fig. 2, whose left panel shows the "forbidden" regions in the Regge plane for selected values of m_b, obtained by requiring that the instability acts on timescales shorter than known spin-up astrophysical processes such as accretion. Here we conservatively require that $\tau_{\rm inst}$ be shorter than the Salpeter timescale for accretion, $\tau_S = 4.5 \times 10^7$ yr. Data points (with error bars) in the left panel of Fig. 2 refer to different observations: (i) Black points denote electromagnetic estimates of stellar and supermassive BH spins obtained using either the Kα iron line or the continuum fitting method [70,71]. (ii) Red points are the 90% confidence levels for the spins of the primary and secondary BHs in (a selection of) the merger events detected in LIGO-Virgo first two runs [72,73]. Here we use the errors on $\chi_{\rm eff} \equiv [(m_1\chi_1 + m_2\chi_2)/(m_1 + m_2)]$ as a proxy for the errors on the individual spins, χ_1 and χ_2. While the binary spins measured so far with GWs are affected by large uncertainties and are anyway compatible to zero for almost all sources (but see [72,73] for a few events in which $\chi_{\rm eff} \neq 0$), future detections will provide measurements of the

individual spins with 30% accuracy [74]. (iii) Green points are the 90% confidence levels for the mass spin of a selection of the GW coalescence remnants [72]. While those events cannot be used to constrain the Regge plane (because the observation timescale is much shorter than $\tau_{\rm inst}$), they identify targets of merger follow-up searches [4,5,9,33,75]. This is particularly important in the spin-2 case, where $\tau_{\rm inst}$ can be as small as a fraction of seconds for typical remnants in the LIGO-Virgo band. (iv) Instead of using τ_S as a reference timescale, more direct constraints would come from comparing $\tau_{\rm inst}$ against the baseline [typically $\mathcal{O}(10\ {\rm yr})$] during which the spin of certain BH candidates is measured to be constant [76], as it is the case for LMC X-3 [77] and Cygnus X-1 [78], shown in the left panel of Fig. 2 by blue points. In particular, Cygnus X-1 can confidently exclude the range $2.9\times10^{-13} < m_b/{\rm eV} < 9.8\times10^{-12}$. (v) Finally, the single gray point is the mass of M87 measured by the Event Horizon Telescope [79,80]. While a direct spin measurement is still not available, M87 has been suggested to have a large spin [81,82]. A putative measurement $\chi_{\rm M87}\gtrsim 0.2$ would constrain the mass range $m_b\sim 10^{-20}-10^{-21}$ eV [83–85]. If the largest known supermassive BHs with $M\simeq 2\times10^{10}\ M_\odot$ [86,87] were confirmed to have nonzero spin [88], we could get even more stringent bounds.

Very precise spin measurements of binary BH components out to cosmological distances will come from the future *LISA* mission [10]. Depending on the mass of BH seeds in the early Universe, *LISA* will also detect intermediate mass BHs, thus probing the existence of ultralight bosons in a large mass range (roughly $m_b\sim 10^{-14}-10^{-17}$ eV) that is inaccessible to electromagnetic observations of stellar and supermassive BHs and to ground-based GW detectors [6,7,76]. This is shown in the left panel of Fig. 2 by the horizonal arrows, which denote the range of projected *LISA* measurements using three different population models for supermassive BH growth [7,92].

Owing to the wideness of the Regge gaps, the range of detectable spin-2 masses is larger than in the scalar case and similar to the vector case. If (spinning) BHs of a few solar masses are detected [93], they can probe $m_b\sim 10^{-10}$ eV, whereas BHs as massive as M87 can reach the other hand of the spectrum, $m_b\sim 10^{-21}$ eV, where ultralight bosons are also compelling dark-matter candidates [16].

Direct GW signatures.—In the right panel of Fig. 2 we compare the GW characteristic strain of Eq. (9) with the characteristic noise strain of current and future GW detectors. For a given boson mass m_b and redshift z, the GW frequency depends very weakly on α, whereas the GW strain is maximum for couplings near the superradiant threshold, $\alpha\lesssim 2M\Omega_H$. Each point in the (nearly vertical) lines corresponds to a single source with a given α at different redshift $z\in(0.001,10)$. Interestingly—owing to the redshift of the frequency—sources at high redshift can emit in the optimal frequency bucket even when their

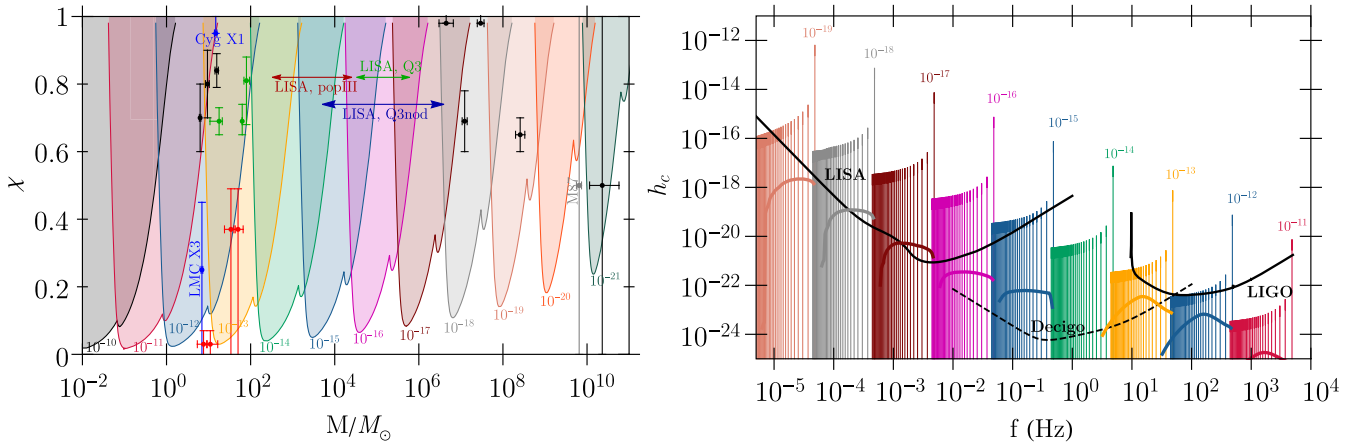

FIG. 2. (Left) Exclusion regions in the BH spin-mass diagram obtained from the superradiant instability of Kerr BHs against massive spin-2 fields for the most unstable quadrupolar ($j=2=m$, $\ell=0$) and octupolar ($j=3=m$, $\ell=1$) modes. For each mass of the field (reported in units of eV), the separatrix corresponds to an instability timescale equal to the Salpeter time, $\tau_S=4.5\times10^7$ yr. The meaning of the markers is explained in the main text. (Right) GW characteristic strain (thin lines) as defined by Eq. (9) for $T_{\rm obs}=4$ yr produced by spin-2 condensates compared to the characteristic noise strain of Advanced LIGO at design sensitivity [89] and to the sky-averaged characteristic noise strain of *LISA* [10,90] (black thick curves). The characteristic noise strain is defined as $\sqrt{fS_n(f)}$, with $S_n(f)$ being the noise power spectral density of the detector. Each (nearly vertical) line shows the strain for a given boson mass m_b, computed at redshift $z\in(0.001,10)$ (from right to left, in steps of $\delta z=0.3$), with α increasing in the superradiant range $(0,2M\Omega_H)$ along each line, and assuming initial BH spin $\chi_i=0.7$. Different colors correspond to different boson masses m_b. Thick colored lines show the stochastic background produced by the whole population of astrophysical BHs under optimistic assumptions [6,7], after subtracting the events that would be resolvable assuming $T_{\rm obs}=4$ yr of coherent observation time. The characteristic noise strain of Decihertz Interferometer Gravitational wave Observatory (*DECIGO*) [91] (dashed line) is also shown for reference.

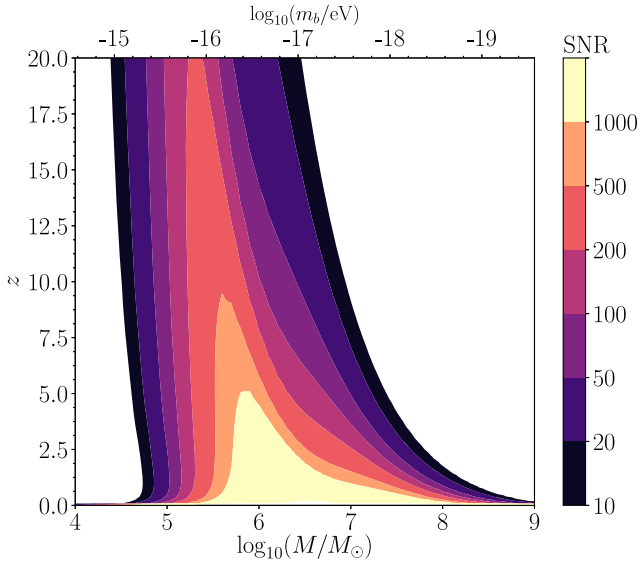

FIG. 3. Waterfall plot [10] showing the angle-averaged *LISA* SNR of continuous GWs from massive spin-2 condensates for different source-frame BH masses and at different redshift. For simplicity we assumed $\alpha = 0.2$, $\chi = 0.7$, and neglected the confusion noise from the stochastic background (see Fig. 2). The SNR is approximately given by $\mathrm{SNR} \sim \sqrt{5} h_c / \sqrt{f S_n(f)}$ (where the factor $\sqrt{5}$ comes from the fact that we are using a sky-averaged *LISA* power spectral density; see, e.g., [94]) and we assumed $T_{\mathrm{obs}} = 4$ yr.

frequency at $z \sim 0$ is marginally detectable. Furthermore, in the *LISA* band, the signal at high redshift decreases more slowly than the slope of the noise, allowing us to potentially detect sources at cosmological distances. This is better shown in the "waterfall" [10] plot in Fig. 3 where we show a typical angle-averaged redshift horizon for *LISA*. Remarkably, the continuous GW signal could be detected even when $z \approx 20$ or higher: every supermassive BH in the Universe with masses $10^{4.5} \lesssim M/M_\odot \lesssim 10^{6.5}$ can potentially be a detectable source if the boson mass is in the optimal range.

Note that LIGO can potentially probe a larger range of spin-2 masses than current bounds from the mass-spin measurements of stellar mass BHs, although the rates for direct GW detections [7], which can provide more stringent constraints, depend on the formation rate of spinning BHs with masses $M \gtrsim 20\ M_\odot$.

Finally, thick solid curves in the right panel of Fig. 2 correspond to the stochastic background from the whole BH population, for a boson mass m_b, computed with the same technique as in Refs. [6,7] and assuming the optimistic BH mass and spin distributions of Refs. [6,7]. Roughly speaking, when the stochastic signal is higher than the detector's noise curve, it produces a "confusion noise," which can complicate the detection of individual sources [6,7]. In the most optimistic scenario, the background would be observable by Advanced LIGO and *LISA* in the ranges $\sim[5 \times 10^{-14}, 10^{-12}]$ and $\sim 5 \times [10^{-19}, 10^{-16}]$ eV, respectively.

To summarize, spin-2 fields with masses $10^{-19} \lesssim m_b/\mathrm{eV} \lesssim 10^{-11}$ (with a small gap around $m_b \sim 10^{-14}$ eV, which might be filled by *DECIGO* [91]) would turn BHs into exotic sources of continuous GWs and of a stochastic background detectable by GW detectors up to cosmological distances.

Our results can be implemented in direct search pipelines for continuous sources, along the lines of axion searches [8,95–97]. Compared to the scalar case, the frequency drift for spin-2 clouds is much faster since $\dot{f}_s \propto \dot{E}_{\mathrm{GW}} \sim \alpha^{4\ell+10}$ is a factor $\mathcal{O}(\alpha^{-4})$ larger than in the scalar case. Thus, spin-2 direct searches can be implemented with the same techniques as in the spin-1 case [33]. In addition, other detection strategies will include follow-up searches of postmerger remnants [5,9,33,75] and self-gravity [98] and tidal effects [99–105] of the condensate in BH binary inspirals. These will require an independent study of the full spectrum of the condensate that is left for the future.

We thank Eugeny Babichev for interesting discussion. R. B. acknowledges financial support from the European Union's Horizon 2020 Research and Innovation Programme under the Marie Skłodowska-Curie Grant Agreement No. 792862. P. P. acknowledges financial support provided under the European Union's H2020 ERC, Starting Grant Agreement No. DarkGRA–757480, and under the MIUR PRIN and FARE programmes (GW-NEXT, CUP: B84I20000100001). The authors would like to acknowledge networking support by the COST Action CA16104 and support from the Amaldi Research Center funded by the MIUR program "Dipartimento di Eccellenza" (CUP: B81I18001170001). This research was supported by the Munich Institute for Astro- and Particle Physics (MIAPP), which is funded by the Deutsche Forschungsgemeinschaft (DFG, German Research Foundation) under Germany's Excellence Strategy—EXC-2094—390783311.

*richard.brito@roma1.infn.it
†paolo.pani@uniroma1.it

[1] A. Arvanitaki, S. Dimopoulos, S. Dubovsky, N. Kaloper, and J. March-Russell, Phys. Rev. D **81**, 123530 (2010).
[2] L. Barack *et al.*, Classical Quantum Gravity **36**, 143001 (2019).
[3] G. Bertone *et al.*, arXiv:1907.10610.
[4] A. Arvanitaki, M. Baryakhtar, and X. Huang, Phys. Rev. D **91**, 084011 (2015).
[5] A. Arvanitaki, M. Baryakhtar, S. Dimopoulos, S. Dubovsky, and R. Lasenby, Phys. Rev. D **95**, 043001 (2017).
[6] R. Brito, S. Ghosh, E. Barausse, E. Berti, V. Cardoso, I. Dvorkin, A. Klein, and P. Pani, Phys. Rev. Lett. **119**, 131101 (2017).

[7] R. Brito, S. Ghosh, E. Barausse, E. Berti, V. Cardoso, I. Dvorkin, A. Klein, and P. Pani, Phys. Rev. D **96**, 064050 (2017).
[8] C. Palomba *et al.*, Phys. Rev. Lett. **123**, 171101 (2019).
[9] M. Isi, L. Sun, R. Brito, and A. Melatos, Phys. Rev. D **99**, 084042 (2019).
[10] H. Audley *et al.* (LISA Collaboration), arXiv:1702.00786.
[11] B. S. Sathyaprakash *et al.*, arXiv:1903.09221.
[12] V. Baibhav *et al.*, arXiv:1908.11390.
[13] M. A. Sedda *et al.*, arXiv:1908.11375.
[14] R. Essig *et al.*, arXiv:1311.0029.
[15] D. J. E. Marsh, Phys. Rep. **643**, 1 (2016).
[16] L. Hui, J. P. Ostriker, S. Tremaine, and E. Witten, Phys. Rev. D **95**, 043541 (2017).
[17] J. Jaeckel and A. Ringwald, Annu. Rev. Nucl. Part. Sci. **60**, 405 (2010).
[18] I. G. Irastorza and J. Redondo, Prog. Part. Nucl. Phys. **102**, 89 (2018).
[19] W. H. Press and S. A. Teukolsky, Nature (London) **238**, 211 (1972).
[20] S. L. Detweiler, Phys. Rev. D **22**, 2323 (1980).
[21] V. Cardoso, O. J. C. Dias, J. P. S. Lemos, and S. Yoshida, Phys. Rev. D **70**, 044039 (2004).
[22] R. Brito, V. Cardoso, and P. Pani, Lect. Notes Phys. **906**, 1 (2015).
[23] Y. Shlapentokh-Rothman, Commun. Math. Phys. **329**, 859 (2014).
[24] T. Damour, N. Deruelle, and R. Ruffini, Lett. Nuovo Cimento **15**, 257 (1976).
[25] T. Zouros and D. Eardley, Ann. Phys. (N.Y.) **118**, 139 (1979).
[26] S. R. Dolan, Phys. Rev. D **76**, 084001 (2007).
[27] P. Pani, V. Cardoso, L. Gualtieri, E. Berti, and A. Ishibashi, Phys. Rev. Lett. **109**, 131102 (2012).
[28] P. Pani, V. Cardoso, L. Gualtieri, E. Berti, and A. Ishibashi, Phys. Rev. D **86**, 104017 (2012).
[29] H. Witek, V. Cardoso, A. Ishibashi, and U. Sperhake, Phys. Rev. D **87**, 043513 (2013).
[30] S. Endlich and R. Penco, J. High Energy Phys. 05 (2017) 052.
[31] W. E. East, Phys. Rev. D **96**, 024004 (2017).
[32] W. E. East and F. Pretorius, Phys. Rev. Lett. **119**, 041101 (2017).
[33] M. Baryakhtar, R. Lasenby, and M. Teo, Phys. Rev. D **96**, 035019 (2017).
[34] W. E. East, Phys. Rev. Lett. **121**, 131104 (2018).
[35] V. P. Frolov, P. Krtous, D. Kubiznak, and J. E. Santos, Phys. Rev. Lett. **120**, 231103 (2018).
[36] S. R. Dolan, Phys. Rev. D **98**, 104006 (2018).
[37] N. Siemonsen and W. E. East, Phys. Rev. D **101**, 024019 (2020).
[38] R. Brito, V. Cardoso, and P. Pani, Phys. Rev. D **88**, 023514 (2013).
[39] K. Hinterbichler, Rev. Mod. Phys. **84**, 671 (2012).
[40] C. de Rham, G. Gabadadze, and A. J. Tolley, Phys. Rev. Lett. **106**, 231101 (2011).
[41] S. F. Hassan and R. A. Rosen, Phys. Rev. Lett. **108**, 041101 (2012).
[42] S. F. Hassan and R. A. Rosen, J. High Energy Phys. 02 (2012) 126.
[43] C. de Rham, Living Rev. Relativity **17**, 7 (2014).
[44] The extension to Einstein spacetimes is straightforward; we assume zero cosmological constant for simplicity.
[45] E. Babichev, L. Marzola, M. Raidal, A. Schmidt-May, F. Urban, H. Veermäe, and M. von Strauss, J. Cosmol. Astropart. Phys. 09 (2016) 016.
[46] See Supplemental Material at http://link.aps.org/supplemental/10.1103/PhysRevLett.124.211101 for a discussion on self-interactions, which includes Refs. [47–49].
[47] T. Ikeda, R. Brito, and V. Cardoso, Phys. Rev. Lett. **122**, 081101 (2019).
[48] H. Yoshino and H. Kodama, Prog. Theor. Phys. **128**, 153 (2012).
[49] H. Yoshino and H. Kodama, Classical Quantum Gravity **32**, 214001 (2015).
[50] R. Brito, V. Cardoso, and P. Pani, Phys. Rev. D **88**, 064006 (2013).
[51] E. Babichev and R. Brito, Classical Quantum Gravity **32**, 154001 (2015).
[52] C. Mazuet and M. S. Volkov, J. Cosmol. Astropart. Phys. 07 (2018) 012.
[53] Incidentally, r_C coincides with the Vainshtein radius within which nonlinearities in massive gravity become important and allow recovering general relativity [43]. However, in our case, this scale emerges already at the linear level.
[54] E. Babichev and A. Fabbri, Classical Quantum Gravity **30**, 152001 (2013).
[55] We explicitly checked that the spherical modes peak at $r \sim r_C$, whereas the special modes peak at $r < r_C$; both families of modes are absent if one neglects the Riemann tensor term in Eq. (2), i.e., they arise from the nontrivial coupling of the two tensor fields.
[56] J. Mathews, J. Soc. Ind. Appl. Math. **10**, 768 (1962).
[57] K. S. Thorne, Rev. Mod. Phys. **52**, 299 (1980).
[58] M. Maggiore, *Gravitational Waves. Vol. 1: Theory and Experiments*, Oxford Master Series in Physics (Oxford University Press, Oxford, 2007).
[59] K. Aoki, K.-i. Maeda, Y. Misonoh, and H. Okawa, Phys. Rev. D **97**, 044005 (2018).
[60] A. A. Starobinskij, Zh. Eksp. Teor. Fiz. **64**, 48 (1973), http://jetp.ac.ru/cgi-bin/e/index/e/37/1/p28?a=list.
[61] A. A. Starobinskij and S. M. Churilov, Zh. Eksp. Teor. Fiz. **65**, 3 (1973), http://jetp.ac.ru/cgi-bin/e/index/e/38/1/p1?a=list.
[62] R. Brito, V. Cardoso, and P. Pani, Classical Quantum Gravity **32**, 134001 (2015).
[63] S. A. Teukolsky, Astrophys. J. **185**, 635 (1973).
[64] H. Yoshino and H. Kodama, Prog. Theor. Exp. Phys. **2014**, 043E02 (2014).
[65] E. Poisson, Phys. Rev. D **47**, 1497 (1993).
[66] G. Ficarra, P. Pani, and H. Witek, Phys. Rev. D **99**, 104019 (2019).
[67] A. Arvanitaki and S. Dubovsky, Phys. Rev. D **83**, 044026 (2011).
[68] K. K. Y. Ng, O. A. Hannuksela, S. Vitale, and T. G. F. Li, arXiv:1908.02312.
[69] N. Fernandez, A. Ghalsasi, and S. Profumo, arXiv:1911.07862.
[70] L. Brenneman, C. Reynolds, M. Nowak, R. Reis, M. Trippe *et al.*, Astrophys. J. **736**, 103 (2011).

[71] M. Middleton, arXiv:1507.06153.
[72] B. P. Abbott *et al.* (LIGO Scientific and Virgo Collaborations), Phys. Rev. X **9**, 031040 (2019).
[73] T. Venumadhav, B. Zackay, J. Roulet, L. Dai, and M. Zaldarriaga, Phys. Rev. D **101**, 083030 (2020).
[74] B. P. Abbott *et al.* (Virgo and LIGO Scientific Collaborations), Phys. Rev. X **6**, 041015 (2016).
[75] S. Ghosh, E. Berti, R. Brito, and M. Richartz, Phys. Rev. D **99**, 104030 (2019).
[76] V. Cardoso, O. J. C. Dias, G. S. Hartnett, M. Middleton, P. Pani, and J. E. Santos, J. Cosmol. Astropart. Phys. 03 (2018) 043.
[77] J. F. Steiner, J. E. McClintock, R. A. Remillard, L. Gou, S. Yamada, and R. Narayan, Astrophys. J. Lett. **718**, L117 (2010).
[78] L. Gou, J. E. McClintock, J. Liu, R. Narayan, J. F. Steiner, R. A. Remillard, J. A. Orosz, and S. W. Davis, Astrophys. J. **701**, 1076 (2009).
[79] K. Akiyama *et al.* (Event Horizon Telescope Collaboration), Astrophys. J. Lett. **875**, L1 (2019).
[80] K. Akiyama *et al.* (Event Horizon Telescope Collaboration), Astrophys. J. Lett. **875**, L6 (2019).
[81] K. Akiyama *et al.* (Event Horizon Telescope Collaboration), Astrophys. J. Lett. **875**, L5 (2019).
[82] F. Tamburini, B. Thidé, and M. Della Valle, Mon. Not. R. Astron. Soc. **492**, L22 (2020).
[83] H. Davoudiasl and P. B. Denton, Phys. Rev. Lett. **123**, 021102 (2019).
[84] Y. Chen, J. Shu, X. Xue, Q. Yuan, and Y. Zhao, Phys. Rev. Lett. **124**, 061102 (2020).
[85] P. V. P. Cunha, C. A. R. Herdeiro, and E. Radu, Universe **5**, 220 (2019).
[86] N. J. McConnell, C.-P. Ma, K. Gebhardt, S. A. Wright, J. D. Murphy, T. R. Lauer, J. R. Graham, and D. O. Richstone, Nature (London) **480**, 215 (2011).
[87] N. J. McConnell, C.-P. Ma, J. D. Murphy, K. Gebhardt, T. R. Lauer, J. R. Graham, S. A. Wright, and D. O. Richstone, Astrophys. J. **756**, 179 (2012).
[88] D. A. Riechers, F. Walter, C. L. Carilli, and G. F. Lewis, Astrophys. J. **690**, 463 (2009).
[89] B. P. Abbott *et al.* (KAGRA Collaboration, LIGO Scientific Collaboration and Virgo Collaboration), Living Rev. Relativity **21**, 3 (2018).
[90] T. Robson, N. J. Cornish, and C. Liug, Classical Quantum Gravity **36**, 105011 (2019).
[91] S. Kawamura *et al.*, Classical Quantum Gravity **23**, S125 (2006).
[92] A. Klein *et al.*, Phys. Rev. D **93**, 024003 (2016).
[93] K. Kyutoku, S. Fujibayashi, K. Hayashi, K. Kawaguchi, K. Kiuchi, M. Shibata, and M. Tanaka, Astrophys. J. Lett. **890**, L4 (2020).
[94] E. Berti, V. Cardoso, and C. M. Will, Phys. Rev. D **73**, 064030 (2006).
[95] L. Tsukada, T. Callister, A. Matas, and P. Meyers, Phys. Rev. D **99**, 103015 (2019).
[96] L. Sun, R. Brito, and M. Isi, Phys. Rev. D **101**, 063020 (2020).
[97] S. J. Zhu, M. Baryakhtar, M. A. Papa, D. Tsuna, N. Kawanaka, and H.-B. Eggenstein, arXiv:2003.03359.
[98] O. A. Hannuksela, K. W. K. Wong, R. Brito, E. Berti, and T. G. F. Li, Nat. Astron. **3**, 447 (2019).
[99] D. Baumann, H. S. Chia, and R. A. Porto, Phys. Rev. D **99**, 044001 (2019).
[100] J. Zhang and H. Yang, Phys. Rev. D **99**, 064018 (2019).
[101] E. Berti, R. Brito, C. F. B. Macedo, G. Raposo, and J. L. Rosa, Phys. Rev. D **99**, 104039 (2019).
[102] D. Baumann, H. S. Chia, J. Stout, and L. ter Haar, J. Cosmol. Astropart. Phys. 12 (**2019**) 006.
[103] D. Baumann, H. S. Chia, R. A. Porto, and J. Stout, Phys. Rev. D **101**, 083019 (2020).
[104] J. Zhang and H. Yang, Phys. Rev. D **101**, 043020 (2020).
[105] V. Cardoso, F. Duque, and T. Ikeda, Phys. Rev. D **101**, 064054 (2020).